Ocean Sci. Discuss., 12, 1729–1764, 2015
www.ocean-sci-discuss.net/12/1729/2015/
doi:10.5194/osd-12-1729-2015

Ocean Science
Discussions
Open Access

Turbulence observations in the Gulf of Trieste under moderate wind forcing and different water column stratification

F. M. Falcieri[1], L. Kantha[1,2], A. Benetazzo[1], A. Bergamasco[1], D. Bonaldo[1], F. Barbariol[1], V. Malačič[3], M. S. Sclavo[1], and S. Carniel[1]

[1]Istituto di Scienze Marine – Consiglio Nazionale delle Ricerche, Venezia, Italy
[2]Colorado Center for Astrodynamical Research – University of Colorado, Boulder, CO, USA
[3]National Institute of Biology, Marine Biology Station, Piran, Slovenia

Received: 17 July 2015 – Accepted: 21 July 2015 – Published: 14 August 2015

Correspondence to: F. M. Falcieri (francesco.falcieri@ve.ismar.cnr.it)

Published by Copernicus Publications on behalf of the European Geosciences Union.

Abstract

During the oceanographic campaign CARPET2014, between 30 January and 4 February 2014, a total of 478 microstructure profiles (grouped into 145 ensembles) and 38 CTD casts were made in the Gulf of Trieste (Northern Adriatic Sea) under moderate wind forcing (average wind speed 10 $m\,s^{-1}$) and heat fluxes (net negative heat flux in the range of 150 to 400 $W\,m^{-2}$). Among the collected profiles, there were three sets of yoyo casts, each lasting for about 12 h for a total of 50 casts. Overall, these represent the first turbulence observations collected in the Gulf of Trieste.

Microstructure profiles collected with a free-falling profiler must be taken in enables of repeated casts, with the objective of obtaining more statistically significant values for turbulence parameters. This approach is certainly feasible in shallow waters, but has a down side when the vertical density structure includes strong interfaces that can move up or down between subsequent casts, under the influence of tides and internal waves. In order to minimize the smearing effect of such interfacial displacements on mean quantities, we developed an algorithm to realign, according to the temperature profile, successive microstructure profiles to produce sharper and more meaningful mean profiles of measured turbulence parameters.

During CARPET2014, the water column in the Gulf evolved from a well-mixed condition to a stratified one, due to Adriatic waters intruding at the bottom along the Gulf's south-eastern coast. These waters stratified the water column and changed its stability characteristics, which in turn prevented wind driven turbulence from penetrating to the bottom of the water column.

In this study, we show that during a warm and relatively dry winter, such as in 2014, the Gulf of Trieste was not completely mixed because of the influence of bottom waters intruding from the open sea, even under moderate wind forcing. Inside the Gulf, two types of water intrusions from the Adriatic Sea were observed during the yoyo casts: one coming from its northern coast (i.e. warmer, saltier and more turbid) and one coming from the open sea in front of the Po Delta (i.e. cooler, fresher and less

OSD
12, 1729–1764, 2015

turbid). Those two intrusions behaved similarly but had a different impact on turbulence kinetic energy dissipation rate profiles. The former, with high turbidity, acted as a barrier to wind-driven turbulence, while the latter, with low sediment concentrations and a smaller density gradient when compared to the rest of the water column, was not able to suppress downward penetration of turbulence from the surface to the same degree.

1 Introduction

In recent years, turbulence and associated processes have gained a broader interest within the ocean sciences community for their fundamental role in many ocean phenomena (Garget, 1997; Thorpe, 2004). Because of their importance in issues such as ocean mixing, energy transfer, dissipation or dispersion of nutrients and pollutants, a better understanding of turbulent processes is paramount for ocean sciences. Yet, direct turbulence measurements in the ocean are still scarce and are not routinely performed. Moreover, when made, these observations are generally not accompanied by auxiliary measurements (such as surface winds, waves and currents) necessary for their interpretation. There is therefore a need to collect more complete datasets suitable for use in the analysis of mixing, and to improve the turbulent mixing parameterization in numerical models.

The Adriatic Sea is an elongated basin (800 km long and 200 km wide, Fig. 1) located in the northernmost part of the Mediterranean Sea. It presents a wide but shallow shelf area (200 km × 200 km and 35 m of average depth) generally referred to as the Gulf of Venice, the first shallow pit system in its central area with the two Pomo depressions with a maximum depth of 260 m and the Southern Adriatic Pit (SAP) that reaches depths up to 1200 m. The water budget is mostly defined by fluxes across the Otranto strait and by inputs of the Po (north-western coast) and Albanian rivers (south-eastern coast) that have significant seasonal variations (Csanady, 1982; Raicich, 1996). Atmospheric forcing is strongly influenced by the surrounding land topography, more specif-

OSD
12, 1729–1764, 2015

ically by the jets of the Bora (a strong seasonal katabatic wind) blowing across the Adriatic Sea from north-east and the Scirocco wind blowing from the south east along the basin main axis (Malačič et al., 1999).

The Gulf of Trieste (GoT) is a small and shallow bay (maximum depth less than 30 m) located in the northeastern corner of the Adriatic Sea. It is generally classified as a region of freshwater influence (ROFI, Simpson, 1997) due to intense riverine discharges, with a marked seasonal variability that strongly influences the general circulation. The second driver of the hydrodynamics of the GoT is wind (Bora and Scirocco) and buoyancy effects of the Isonzo river plume. Bora winds generate a cyclonic circulation in the northern Adriatic and push surface waters out of the GoT, inducing a compensating inflow of open sea water near the bottom (Malačič et al., 2012). The inflow/outflow transport is governed by topographic control of the wind-driven circulation (Csanady, 1982). During Scirocco winds however, the water masses at the surface are driven to the northern shore of the Adriatic Sea between Venice and Trieste, where they bifurcate in front of the GoT. The eastern side of flow turns right and enters the GoT along its northern coastline, while the western side turns left and contributes to the coastal current flowing towards the Venice lagoon (Malačič et al., 2012).

The Isonzo river plume, during windless conditions, occupies the surface of the northern GoT with inertial motions near the river outlet resulting in a quasi-geostrophic motion and a convergence zone along the frontal line that embraces the plume's bulge (Malačič et al., 1999). Due to vertical mixing of surface fresh water with sea water across the halocline, this plume induces the inflow of water masses near the bottom of the GoT (Malačič and Petelin, 2001). The Isonzo plume and its variability play a fundamental role in driving the bottom circulation of the GoT. The annual mean flow rate between 1998–2005 was around 90 $m^3 s^{-1}$ (Comici and Bussani, 2007), but different estimates, varying by a factor of three from this value, can be found in literature. In January–February, the monthly mean flow rate in 1998–2005 ranged from 1 to 351 $m^3 s^{-1}$, with 41 $m^3 s^{-1}$ on the average (Comici and Bussani, 2007). In 2014, the Isonzo river experienced a period of strong discharges, with February 2014 average

OSD
12, 1729–1764, 2015

discharge rising to 547 $m^3 s^{-1}$. During the sampling period inside the GoT, the mean discharge was 868 $m^3 s^{-1}$ with maximum and minimum values of 1768 and 327 $m^3 s^{-1}$ respectively (according to data collected from the "Servizio Idrometereologico – Protezione Civile Friuli Venezia Giulia").

Turbulence measurements in the Adriatic Sea are scarce and scattered. By far, the largest number of available casts is retained by the "Istituto di Science Marine – Consiglio Nazionale delle Ricerche" (CNR-ISMAR), with more than a thousand quality-controlled samples, ranging from a few meters to over 900 m in depth. To our knowledge, a very limited number of papers dealing with this topic have been published in literature. Peters and Orlić (2005) presented the first measurements of turbulence in the Adriatic Sea with a set of 32 casts in the central basin collected in May 2003 within the framework of the DOLCEVITA project. During the collection period, wind forcing was weak and the water column generally well stratified with a shallow mixed layer depth. The authors found small values for the turbulent kinetic energy (TKE) dissipation rates in the upper mixed layer. Peters et al. (2007) reported a second set, collected in February 2003 within the DOLCEVITA project in the shallow northern Adriatic under strong winds, intense cooling and a well-mixed water column. Their data consist of seven microstructure stations and two deployments of a bottom lander with an upward looking ADCP. Their main findings highlight different contributions of surface forcing and bottom friction on the TKE dissipation rate profiles. At both study sites, the main contribution to turbulence generation was found to be mechanical rather than buoyancy effects.

Carniel et al. (2008) discussed two sets of repeated observations (for a total of 47 casts) in the southern Adriatic Sea in front of the Gargano peninsula during the March 2006 DART06A cruise. Their microstructure studies revealed layered thermohaline staircase structures that originated from double diffusive convection. During the DART06B cruise (August 2006), Carniel et al. (2012) collected the most comprehensive turbulence data set published to date for the Adriatic Sea. A total of more than 300 casts allowed the authors to describe the upper oceanic mixed layer under a series

OSD
12, 1729–1764, 2015

of different meteorological conditions (different wind forcing, night-time convection and strong insolation).

A set of microstructure observations with a free-falling probe has been collected in June 1990 by J. Imberger with the support of Marine Biology Station (NIB-MBS) in Piran, but at the time of publication of this article that data set is still unpublished.

All of the studies cited above deal almost exclusively with the surface mixed layer and only in Peters et al. (2007) there is a discussion of the role of the bottom boundary on turbulent dissipation rates. This means that the interaction between surface and bottom turbulence has only been described briefly in the Adriatic Sea.

However, two recent sets of observations deal with the role of the sea floor and its influence on turbulence and sediment transport. The first set (currently under publication) was collected over a field of mud waves in spring 2013 in southern Adriatic during the DECALOGO2013 campaign on board R/V *Urania*. During the cruise, TKE dissipation rates were documented in four transects over a field of mud waves located in the Southern Adriatic Shelf edge, an area that is influenced by the Northern Adriatic Dense Water.

In this paper, the observational data from the CARPET2014 campaign will be described. Operations on-board the R/V *Urania* in the northern Adriatic Sea between the 29 January and the 10 February will be described.

2 Measurements and data processing

The CARPET2014 turbulence data set was collected in the winter of 2014 in the GoT and in front of the Po river Delta (Fig. 1) using two microstructure (MSS) profilers. Each cast was made by dropping the MSS profiler in free fall and recording physical parameters until the probe hit the sea floor. This operational procedure permitted collection of observations close (8 cm from the bottom) to the sea floor. During the cruise, 818 casts were collected at 104 stations, 554 with a MSS profiler owned by ISMAR-CNR and 264 with the NIB-MBS profiler. At each station, three to five profiles were measured, then

OSD
12, 1729–1764, 2015

all of each station's casts were averaged to obtain a mean profile representative of the water column condition during sampling. We will refer to these profiles as ensemble casts.

Among all the stations, 3 were in yoyo mode. By yoyo mode, we mean a series of repeated casts in a fixed location with the R/V either at anchor or dynamically keeping the position. A yoyo series is helpful in studying the temporal evolution of the water column at a fixed location, but at the loss of synoptic and spatial information. A subset of the collected observations will be used in this paper, more specifically the casts collected inside the GoT between 30 January and 4 February. The three yoyo casts were made at two locations close to each other in the deepest part of the GoT (blue squares in right panel of Fig. 1) with a sampling rate of 30 min. The first yoyo set (Y01) is composed of 11 casts (from Y01-01 to Y01-11) starting on 30 January at 20:50 UTC and ending on 31 January at 02:30 UTC; the second set (Y02) has 12 casts (Y02-01 to Y02-12) from 1 February at 14:00 UTC to 2 February at 01:40 UTC; the last set (Y03) has 27 casts from 3 February at 15:50 UTC to 4 February 04:11 UTC. During the last part of Y03, the sampling frequency was increased to every 15 min.

Ancillary observations include 104 CTD casts with SBE 911, current measurements were made with a downward looking hull-mounted ADCP (RDI workhorse 75 Khz, acoustic bin size set to 4 m with a blank interval of 5 m and first bin centred at 7 m), and meteorological forcing was acquired by the R/V *Urania* hull-borne weather station and by the NIB VIDA buoy.

2.1 Meteorological conditions and surface forcing

Winter 2013–2014, compared to the climatological mean, can be considered to be dry and warm with light rain and wind. But January 2014 and the period of the CARPET2014 cruise were anomalously warm and moist. During the campaign, there was a warm and moist air mass flowing from the southeast (northern coastline of Africa) over the northern Adriatic region and Dinaric mountain ridge that constitutes the north-eastern corner of the Adriatic Sea. At the same time, a cold water mass was flowing

OSD
12, 1729–1764, 2015

from the eastern part of the European continent towards the northern Adriatic Sea. A strong temperature inversion was present at around 1000 m altitude, where over a thickness depth of 400 m, the air temperature increase with height was 8 °C, as revealed by a balloon sounding over Ljubljana in the early morning of 2 February 2014 (Sinjur et al., 2014). In the northeastern landscape of the Adriatic Sea, this weather constituted an extreme sleet hazard in Slovenia, which was struck by a severe ice storm.

Atmospheric data, sea surface temperature and salinity (Fig. 2, left panel) were recorded throughout the cruise from the R/V *Urania*'s ship-borne weather station (located about 10 m a.s.l.) and by a thermistor and a salinometer mounted on the R/V hull, about 2 m below sea level. The latter, when compared to CTD data, presents a bias of 0.2 psu, and hence its measurements used for computation of fluxes, were corrected for bias. The R/V *Urania* sailed in the GoT and did not hold a fixed position, and therefore, in order to have a complete representation of the atmospheric conditions, the ship-borne weather observations need to be supplemented by a fixed observation point. Data collected from the Slovenian coastal observatory VIDA were then also used for computation of fluxes (Fig. 2, right panel). The VIDA buoy is anchored at a depth of 22 m about 2.3 km off the coast in front of Piran (www.nib.si/mbp/en/buoy). Atmospheric observations and fluxes computed using the two datasets are strongly similar. Hence their merged analysis can be considered as representative of the atmospheric conditions over the whole GoT during the campaign. The small scale variations in R/V *Urania*'s dataset have to be ascribed to a higher sampling rate (one record per minute) averaged over 10 min intervals used for flux computations, compared to the 30 min averages of the VIDA buoy.

Wind observations taken from R/V *Urania* and at VIDA buoy are very similar (Fig. 2b). At the beginning of the measurements, easterly Bora was turning to south-east Scirocco (about 10 m s^{-1}) that lasted for two days until the night of 2 February, when it turned back to Bora with wind speeds above 10 m s^{-1}. During the Scirocco event, three calm periods were recorded with weak winds from north. Air temperature shows a sim-

OSD
12, 1729–1764, 2015

ilar pattern with lower values during Bora (between 5 and 8 °C), a warmer one during Scirocco (up to 14.5 °C). The three calm periods can also be seen in air temperature, with sudden drops of about 5 °C. Throughout the cruise, sea surface temperature was rather constant around 11.5 °C with an increasing trend toward the end of the operations (Fig. 2a). The ship-borne observations show a stronger variability with respect to the VIDA ones due to the R/V positional changes within the GoT. Analogous behaviour can be seen in sea surface salinity (not shown).

Figure 2c shows the heat fluxes computed using the COARE algorithm (Fairall et al., 2003), from on site-observations (sea surface temperature and salinity, air temperature, pressure and humidity) and from short and long wave radiation. The radiation fields are derived from an implementation of the Coupled Ocean Wave and Sediments model over Centre Europe with a 7 km horizontal resolution (Ricchi et al., 2015).

Net heat flux is always negative at both sites, with a heat loss from the ocean to the atmosphere always higher than 150 $\mathrm{W\,m^{-2}}$ during Bora events (peaks of just over 400 $\mathrm{W\,m^{-2}}$ at *Urania* and 350 $\mathrm{W\,m^{-2}}$ at VIDA). During Scirocco events, fluxes were generally smaller, with heat losses in the range of 100 $\mathrm{W\,m^{-2}}$. It is noteworthy that on the one hand the latent heat flux is always negative, but on the other hand, sensible heat flux turns positive during Scirocco due to air temperature being higher than the sea surface. This is not the case during the three calm periods, when a drop in wind speed and air temperature below sea temperature result in a switch in the sensible heat flux direction.

The buoyancy flux at the surface (Fig. 2d) was obtained following Shay and Gregg (1986, 1984) as:

$$J_\mathrm{b} = \frac{g}{\rho_w}\left\{\frac{\alpha}{C_p}J_\mathrm{t} + \frac{BS}{L_\mathrm{E}(1-S)}J_\mathrm{l}\right\} \quad (1)$$

in which the first term inside brackets represents the heat buoyancy flux, computed from the net heat flux (J_t), the thermal expansion coefficient ($\alpha = -2.16 \times 10^{-3}\,^\circ\mathrm{C}^{-1}$) and the sea water specific heat ($C_p = 3.98 \times 10^{-4}\,\mathrm{K}^{-1}$), while the second one shows

OSD
12, 1729–1764, 2015

the evaporative buoyancy flux computed from the latent heat flux (J_l), the haline contraction coefficient ($\beta = 0.79$), the latent heat of evaporation ($L_E = 2.6 \times 10^6\,\mathrm{J\,Kg^{-1}}$) and sea surface salinity expressed as concentration. The convention used for heat and buoyancy fluxes in this study is that negative/positive fluxes correspond to losses/gains from/to the ocean to/from the atmosphere. In the case of buoyancy, this means that a negative J_b corresponds to a loss of buoyancy from the ocean to the atmosphere (i.e. water is getting less dense) with a stabilizing effect on the water column, while positive J_b indicate a gain of buoyancy (i.e. water becoming less dense) and hence a destabilizing effect on the water column.

2.2 Microstructure measurements and processing

The temperature and salinity measurements from the two MSS probes were calibrated against CTD observations by pairing the first cast of each MSS ensemble to its spatially ad temporally closest CTD. Of all possible pairings, only those that were closer than 1000 m and taken less than 15 min apart were considered. In order to have an optimal cross calibration, all profiles with a stratified water column were ignored (i.e. those profiles that presented a salinity range higher than 0.3 PSU or a temperature range higher than 0.5 °C). This was necessary because in the presence of a thermocline or halocline, even a small vertical displacement (due to interface oscillations) between casts could result in measures of different values at the same depths and hence errors in calibration.

The bias, root mean squared error (RMSE) and percentage root mean squared error (PRMSE) of each pair were computed, and all profiles with PRMSE less than 1 % were used to compute each sensor bias. Results are shown in Table 1.

Among all the profiles collected by the ISMAR probe, 73 pairs were identified following spatial and temporal proximity criteria and 21 were selected for cross calibration based on vertical stratification criterion. The NIB probe had 60 pairs and 28 of those eligible for calibration. For all profiles the BIAS and RMSE are very low, almost at the precision limit of each sensor, and PRMSE values are therefore small. The only sen-

OSD
12, 1729–1764, 2015

sor that shows a significant BIAS (−0.2418 PSU) is the salinity sensor on the ISMAR profiler, which was therefore corrected for later computations.

Shear data from both profilers were used to determine the turbulent kinetic energy dissipation rate (ε), the dissipation rate of temperature variance (χ), eddy (K_ρ) and heat diffusivity (K_h) and the Thorpe scale (L_T). The surface data up to 5 m depth (two times the draft of the ship) of each cast were not considered in the analysis due to contamination from R/V *Urania*.

The traditional approach to reach statistical significance and increase the accuracy calls for averages of repeated casts (in practice, three or more) at each station. The averaging produces meaningful results for the mean profiles and yields quantities more representative of the turbulence in the water column. However, cases in which the water column has strong stable density interfaces moving up and down are exceptions. In those cases, turbulence and other parameters differ from one cast to another in their vicinity. In the CARPET 2014 dataset, changes in the interface depth between casts are as much as 4 m. This means that by averaging measured quantities at fixed depths over consecutive profiles, the averages are smeared, and hence characterized by smoother gradients and broader peaks. To avoid this, an algorithm was developed using the central profile of each ensemble as reference and realigning sections of the remaining profiles to it. The mean profile was then obtained by averaging the central profile with the realigned sections. The step-by-step procedure applied to two vertical profiles, is as follows:

1. One profile is chosen as the reference (Fig. 3a, cyan) and the other as the one to be realigned (Fig. 3a, black).

2. Starting from the surface the correlation coefficients are computed for a progressively longer section, until the full profiles (i.e. surface to bottom) are accounted for. Starting from the surface, the section with the maximum correlation value is considered as a "surface layer" that does not need to be shifted. In Fig. 3b, its lower limit is the horizontal red line.

OSD
12, 1729–1764, 2015

3. The root mean square error for remaining parts of the profiles is then computed with a 5 point moving window (Fig. 3c, red line) and the maximum peaks are found (Fig. 3c, red dots), if two peaks are closer than 10 points to each other, just the largest one is considered. The 10-point window was chosen because in a sensitivity test (not shown), it proved to be the most efficient in separating two peaks. The two peaks are then used to identify the sections to realign. The limit of each section is set at the midpoint between two peaks (Fig. 3, black lines).

4. Each section of the profile to be realigned is then correlated to the reference profile shifting it from +20 to −20 points. The shift with maximum correlation is then taken as the needed shift. In Fig. 3d, the reference profile is in cyan, the one to be shifted in black and the shifted sections are in red.

The process is repeated for each successive cast at the station and then the averages are computed over the new shifted profiles and the reference one. Figure 3 shows the original profiles (left panel, red: reference, green: profile one and blue: profile 3), their conventional mean in black, the shifted profiles and their mean (central panel, same colours) and the two means (right panel, original mean in cyan and shifted mean in black). Figure 3 presents the same plots but for ε.

The method described above offers a more meaningful vertical distribution of the TKE dissipation rate, by taking into account the vertical oscillations of the pycnocline, since turbulence is extinguished in the vicinity of strongly stable interfaces. As a consequence, in the vertically shifted profiles, the peaks in the TKE dissipation rate are much clearer. The peaks are just above the thermocline. In general, when more than one cast is collected at a station, the most conservative assumption is to consider the central profile as the reference one for the water column structure. Other profiles over the cycle are then realigned with respect to the reference profile to obtain the TKE dissipation rate caused by vertical shear, uncontaminated by the zero values right at the interface.

OSD
12, 1729–1764, 2015

The TKE profiles collected will be analysed by employing a similarity scaling (Sect. 3.2) to relate the turbulence dissipation rate (ε) to mechanical forcing (i.e. wind stress, bottom shear stress) and buoyancy driven turbulence generation (Peters et al., 2007). The goal of this approach is to identify the dominant forcing and to highlight discrepancies between the theoretical and the observed profiles in order to identify sites in which the dissipation rate differs from that expected due to the presence of buoyancy interfaces such as a pycnocline or due to changes in suspended sediment concentration. It is generally accepted that mechanical generation of turbulence due to surface wind stress (ε_s) follows a law of the wall relationship for which

$$\varepsilon_s = \frac{u_*^3}{k|z|} \tag{2}$$

with friction velocity given by

$$u_* = \sqrt{\frac{\tau_a}{\rho}} \tag{3}$$

where τ_a is the surface wind stress and $k = 0.4$ is the von Kàrmàn constant.

Likewise turbulence generated by bottom shear stress scales as

$$\varepsilon_b = \frac{u_{*a}^3}{k|h|} \tag{4}$$

with bottom friction velocity

$$u_{*b} = \sqrt{\frac{\tau_b}{\rho}} \tag{5}$$

where τ_b is the bottom shear stress. The currents measured by the ADCP in the cell closest to the sea floor were used to compute the bottom stress. For Y02 and Y03

OSD
12, 1729–1764, 2015

series, this means that current observations are the average of a cell that span from 13 to 17 m depth, which is roughly 8 m above the sea floor. Hence the bottom stress computed using a drag coefficient of 0.003 and quadratic drag law needs to be regarded as just a rough estimation.

Given that the surface buoyancy flux J_b and ε have the same dimensions, it can be shown that for oceanic convection in surface mixed layer, the TKE dissipation rate due to buoyancy flux can be expressed as $\varepsilon_b \sim 0.6 J_b$ (Shay and Gregg, 1986; Peters et al., 1988).

3 Hydrological conditions and water mass structure

During the sampling period, the GoT was subject to moderate wind forcing, with an average wind of over 10 m s^{-1} and peaks of 16 m s^{-1}, starting with Scirocco from 30 January to 1 February and then Bora winds. During the Scirocco period, two calm wind periods with velocities below 2 m s^{-1} can be observed (Fig. 2). The result of this type of forcing on the GoT is a combination of wind-driven circulation during two prevalent winds (as pointed out in the introduction), with inertial oscillations in offshore areas where those winds prevail, during times of wind shifts from the one type to another and during period of calms between windy episodes.

Weather and ship logistical constraints did not permit a synoptic hydrological survey of the entire GoT. Instead, different parts of the basin were covered each day. In order to give a rough overview of the hydrodynamics of the GoT, surface (from 0 to 2.5 m) and bottom (last 2.5 m of cast) temperature and salinities collected on 30 and 31 January, and 4 February from CTD casts are shown in Fig. 4 along with the bottom currents measured by hull-mounted ADCP.

The overall picture emerging from Fig. 4 is a bottom circulation with waters incoming from the open sea along the southeastern coast and flowing out along the northwestern one (left panels). The same pattern is common to both tidal intervals, during rising (red arrows in Fig. 4 left panels) and falling (Fig. 4, left panels, blue arrows) tides, with

OSD
12, 1729–1764, 2015

the latter showing weaker currents. The intervals of rising and falling tides have been defined from the pressure values recorded by the bottom mounted ADCP located at the VIDA buoy. The apparently incoherent vectors close to the coast can be explained by the influence of the coastline and of the shallow topography on the local currents. Each plot shows a 24 h collection of data over a relatively small area, and hence can also include small-scale variations.

Temperature and salinity distributions (Fig. 4) are in agreement with the general picture of warmer and saltier bottom waters entering the southern part of the GoT and cooler and fresher waters confined in the northern part. The low surface salinity values in the northernmost part and in front of Trieste (Fig. 4, right panels) are the result of the influence of the Isonzo and Timavo discharges (Fig. 1, left panel), respectively. It is of interest to note that on 4 February, the easternmost stations are warmer and saltier throughout the water column than those on 30 January. This cooling of the water column is due to the constant negative heat flux between Y02 and Y03 (Fig. 2).

The θ–S (potential temperature – salinity) plot in Fig. 5 helps in identification of the water masses that were present in the GoT and in the Northern Adriatic Sea during the operations from the CTD and MSS surveys. Inside the GoT (Fig. 5, dark grey dots), the water temperature was lower than that in the outside of the basin (Fig. 5, light grey dots), due to the moderate negative net heat flux throughout the cruise (ranging between -150 to $-400\,\mathrm{W\,m^{-2}}$) and the shallow bathymetry of the GoT. Apart from the Isonzo river mouth and the inner part of the Gulf, salinity shows values comparable to (or just short of) the rest of the Adriatic Sea. By looking at Y02 and Y03 casts (Fig. 5, red and green dots), it is possible to highlight the different origins of the bottom waters. More specifically, yoyo series Y02 presents deep waters (Fig. 5, dark green) whose θ–S values are directed towards an end point (green circle in Fig. 5, location shown in Fig. 1, right panel) close to the density isoline $1029\,\mathrm{kg\,m^{-3}}$, compatible with fresher, cooler and more turbid waters (Fig. 5, right panel) observed right outside the GoT on 30 January typical of Northern Adriatic coastal waters. On the other hand, yoyo 03 (Y03) θ–S values of bottom waters have an end-point (red circle in Fig. 5,

OSD
12, 1729–1764, 2015

location shown in Fig. 1 right panel) typical of the open basin, slightly warmer, saltier and cleaner waters (Fig. 5, right panel). Moreover, in the case of Y03 end-point, its characteristics are similar to the open sea bottom waters in front of the Po Delta (Fig. 5, left pane black square). The slight misalignment of those θ–S points with respect to the Y03 endpoint can be explained by their position being still close to the influence of the Po river plume. Both end points are located over the same station but were recorded four days apart, the first one on 31 January and the second one on 4 February.

4 Yoyo casts and turbulence observations

Yoyo cast Y01 is in a shallower part of the GoT closer to the coast (Fig. 1, red square in left panel). It presents a well-mixed water column with no visible stratification and just a small increase in temperature (less than 0.2 °C) and a decrease in salinity (about 0.1 psu) toward the end of the yoyo series (Fig. 6). During sampling, with surface salinities are over 37 psu, surface data show no influence of the Isonzo river. The turbidity levels, however, were significantly high, in the range of 22.6 to 23.5 FTU. TKE dissipation rate profiles show high values near the sea surface, which progressively decrease to values of the order of $10^{-6}\,\mathrm{W\,kg^{-1}}$ near the bottom, with one exception being the cast Y01-05 in which ε values are high throughout the water column. ADCP measured currents (Fig. 7, lower panel green line) show generally low bottom currents of magnitudes below $0.1\,\mathrm{m\,s^{-1}}$ with an increase toward the end of observations to values just short of $0.2\,\mathrm{m\,s^{-1}}$. This can be explained by the change in tidal regime from falling to rising tide and is also reflected in the ε profiles that show an increase near the sea floor for the last ensembles of the series (Fig. 8). The shallower cell (Fig. 7, upper panel green line) presents a similar condition, with two peaks of magnitude just short of $0.2\,\mathrm{m\,s^{-1}}$ but without an increase during sampling. Current directions (Fig. 7, black lines) are more complicated, with dominant direction from the east for the surface cell, and from the southwest for the bottom cell.

OSD
12, 1729–1764, 2015

The TKE dissipation rate profiles support measurements just described and are also in agreement with the local forcing (Fig. 8). In the case of Y01-01 and Y01-07, characterized by stronger wind forcing, dissipation rates fall around $10^{-6}\,\mathrm{W\,kg^{-1}}$ at around 8 m depth, while the bottom shear stress does not seem to influence the TKE dissipation rate much. The Y01-08 ensemble was under weak winds and the resulting TKE dissipation rate reaches low values at shallower depth, just below 5 m. The last ensemble of the series (Y01-11) was collected during rising tide with bottom currents up to $0.2\,\mathrm{m\,s^{-1}}$ and moderate wind stress. This is reflected in the TKE dissipation rate profile with a decrease with depth in the first 10 m and then an increase in the last 5 m, due to the influence of turbulence generated by the bottom shear stress. In all cases, the contribution of buoyancy-generated turbulence is weak (ε_b, magenta dashed line in Fig. 5). Y01 profiles show that in the absence of water column stratification, the ε profile is defined by the surface wind and bottom stresses. In this case, the turbulence generation due to buoyancy can be neglected, since the buoyancy flux is low and the Monin–Obukhov length scale is very large (negative) and larger than the local sea floor depth (Fig. 2d).

Yoyo casts Y02 and Y03 are located at the same site (Fig. 1) but roughly two days apart from each other and therefore present significant differences in both water column structure and ε profiles. Water column observations collected during Y02 (Fig. 9) show a change in stratification, from a condition with colder and fresher waters at the surface (coherent with the influence of the Isonzo river discharges, as supported by high turbidity) to a condition with warmer and saltier water masses near the sea floor. Suspended sediment concentrations increase at bottom at the beginning and towards the end of the yoyo. Apart from the surface layer, TKE dissipation rate is low at mid-depths with values almost at noise level (ε values lower than $10^{-8}\,\mathrm{W\,kg^{-1}}$) but increases by two orders of magnitude around 18:00 UTC of 1 February and then again decreases to very low values. ADCP currents (Fig. 10) at bottom (ADCP cell 3 centred at 13 m depth, lower panel) and mid depths (ADCP cell 2 centred at 9 m depth, top panel) are similar with water flowing to the northeast during a rising tide up to around 20:00 UTC with

OSD
12, 1729–1764, 2015

currents reaching 0.2 m s^{-1}. Once the tidal phase changes to falling tide, currents turn toward southeast, with a pronounced change in the bottom layer, and drop to values below 0.05 m s^{-1}.

In contrast to the Y01 set, Y02 ensembles have a more complex behaviour due to the presence of surface stratification, the incoming water mass and the change in tidal character. The first ensemble casts Y02-01 and Y02-04 (Fig. 8, middle panels) have a similar water column structure, with fresher and cooler waters at the surface and more turbid waters near the sea floor. The surface wind stress is weak during both casts and a steep drop of ε to values below 10^{-6} W kg^{-1} can be seen around 7 m depth. Below this depth, the two ε profiles diverge due to different bottom current velocities. In Y02-01, ε falls to noise level due to a much slower bottom current (and hence low bottom shear stress) and higher turbidity that damps wind-generated turbulence. In contrast, in Y02-04, TKE dissipation rate was significantly higher, reaching values above 10^{-6} W kg^{-1} with a profile that follows closely the ε_{sb}. In the second half of the yoyo series, wind speed increased up to values around 10 m s^{-1} which results in a deepening of the ε drop from 7 to 10 m and 15 m in Y02-06 and Y02-10 respectively. Y02-06 has a bottom current velocity close to that of Y02-04, but the resulting ε reaches lower values at the bottom.

A more extreme case of an abrupt drop in TKE dissipation rate near the sea floor is Y02-10, in which ε reaches noise levels just 5 m above the sea floor. This is the result of concurrence of two factors. On the one hand, a sudden drop in bottom current velocity can be related to the change in the tidal character (that results in a lower ε_{sb}). On the other hand, a different water mass (warmer, saltier and with high concentrations of suspended sediments) intrudes in the bottom layer and acts as a physical barrier to the propagation of wind-generated turbulence to the bottom part of the water column. The turbulence generated by buoyancy flux is low throughout yoyo Y02 with the exception of the first ensembles, as shown by the Monin–Obukhov length (Fig. 2).

Y03 (Fig. 9, right panels) presents a water column colder and fresher than Y02 with values closer to Y01. There is no surface salinity stratification as a result of strong

OSD
12, 1729–1764, 2015

Bora winds that enhance vertical mixing and tend to push the Isonzo plume out of the GoT along its northern shore. Moreover, the Isonzo discharges during Y03 presented a temporary decrease in magnitude from the massive flood event. The mean discharge between noon of 3 and 4 February was 500 $m^3 s^{-1}$. Near the sea floor, two intrusions are visible (both in temperature and salinity); one right at the beginning of the series ending at about 16:00 UTC, and one starting around 00:00 UTC and lasting for the remaining part of the yoyo. Even though those intrusions involve water masses of similar temperature and salinity, they are significantly different in turbidity, with the first intrusion being more turbid than the second one. This can be partially ascribed to current speed and direction, with the first intrusion flowing south-west at velocities higher than 0.1 $m s^{-1}$ and the second one due east at a much lower speed (Fig. 10). Considering water mass characteristics, the second intrusion shows water masses that are coherent with an open sea origin as shown in Fig. 5. It is of interest to note the abrupt change in current direction around 00:00 UTC right at the beginning of the second intrusion, which also points toward a different origin of this water mass.

Y03 turbulent kinetic energy dissipation rates are higher than those of Y02 throughout the series. Y03-01 presents a water column that is similarly stratified as that during Y02-10 (gradients across the pycnocline were of similar magnitude), with a mixed surface layer and with intruded turbid and dense water at bottom. Below the mixed surface layer, the ε value drops to almost 10^{-8} $W kg^{-1}$ at the top of the intrusion (20 m) and then abruptly rises back to values of the order of 10^{-6} $W kg^{-1}$ as a consequence of high bottom currents (Fig. 8). In the case of Y03-07, there is no intrusion and hence no pycnocline, so that the ε profile after decreasing in the surface layer stays in the range of 10^{-6} $W kg^{-1}$ throughout the water column. In the second part of the yoyo series (Y03-18 and Y03-20), the arrival of the intruding water mass develops a density that, in contrast to Y03-01 and Y02-10, is not enhanced by a high suspended sediment load and hence the TKE dissipation rate is damped to a lesser degree than in the other cases.

OSD
12, 1729–1764, 2015

5 Summary and discussion

Between the end of January and the first week of February 2014, during a period of high river discharges and moderate wind forcing, we were able to collect the very first microstructure measurements in the Gulf of Trieste. These observations, along with CTD casts, ADCP currents and meteorological measurements, provided a comprehensive picture of the effect of different forcing and water masses on the penetration of turbulence from its source regions and therefore, on mixing in the water column.

The θ–S diagram (Fig. 5) shows that the GoT has salinity values close to or just smaller than those of the Northern Adriatic Sea waters, even during a period of high discharge of the Isonzo river. This can be explained by the interaction between different forcings: (i) the moderate Scirocco and Bora winds that tend to keep the plume confined to the northern coast and push it due west, outside the Gulf, (ii) the generally negative heat fluxes (from -150 to $-400\,\mathrm{W\,m^{-2}}$), that result in a net buoyancy loss from the sea surface (Benetazzo et al., 2014), (iii) the vertical mixing inside the GoT that, in absence of intruding water masses, tends to keep the water column mixed.

The general circulation of the GoT is cyclonic with waters entering the Gulf from its southeastern coast and outflowing along the northern shore. The bottom waters observed during Y02 and Y03 have different end points, a condition that suggests two different origins. In the case of Y02, higher temperature and turbidity observed are consistent with waters coming from the northern coast of the Adriatic Sea, while clearer and colder waters of Y03 have an open sea origin. It is important to note that, even though the two origin sites are close to each other, these two water masses have different physical characteristics and so have a different impact on the turbulent kinetic energy dissipation rate profiles once they enter the GoT.

In the period covered by observations, the GoT was subject to moderate winds, with two calm periods in-between and a change in wind direction from southwestern Scirocco to northeastern Bora, and moderate heat fluxes (Fig. 2). Bottom circulation appears to be influenced by winds both in magnitude and direction: during strong winds

OSD
12, 1729–1764, 2015

periods, such as during Y02 or the beginning of Y03, bottom currents increase in magnitude, while during weaker winds, such as the beginning of Y02 and the end of Y03, they tend to decrease (Fig. 10). Bottom current velocities are also influenced by tidal phases with rising tides having an enhancing effect, as shown by the marked decrease at Y02 right after the tidal change, even under wind forcing in the order of $10\,m\,s^{-1}$ (Fig. 4).

TKE dissipation rates follow closely the similarity scaling for wind stress generated turbulence and for the one due to bottom shear stress near the sea floor (Fig. 8). Buoyancy-driven turbulence under those conditions proved to be generally not significant, as also shown by the Monin–Obukhov length scale, which is almost always greater than the sea floor depth. The behaviour of the dissipation rate under stronger heat fluxes, such as those observed in February 2012 (Benetazzo et al., 2014), could be significant, but has not yet been investigated.

Turbulence dissipation rate profiles throughout the campaign indicated values higher than $10^{-6}\,W\,kg^{-1}$ in the near-surface layers, then decrease up to two order of magnitude in the mid water column. In casts with strong bottom currents (i.e. Y01-11 or Y02-04), with the exception of the intrusion in Y02, dissipation rates tend to increase back to values of $10^{-6}\,W\,kg^{-1}$ near the sea floor due to the bottom stress. Anyway, this is a feature that has not been observed in the Adriatic Sea, mostly because observations used in previous studies did not reach the sea floor.

In our observations, apart from surface and bottom stresses, the water column structure (both the presence of buoyancy interfaces and suspended sediments) proved to be also important in determining the TKE dissipation rate. The profiles collected during the three yoyo casts can help in drawing a general picture. The first yoyo cast (Y01) shows a simple condition with a well-mixed water column, no interfaces and moderate wind forcing. Under these conditions, TKE dissipation rate profiles are defined mostly by the surface and bottom stresses, and turbulence can penetrate into the water column. Under weak bottom currents, such as at the beginning of Y01 series (Fig. 7), ε profiles generally show a linear decrease from the sea surface to about 8 m (Fig. 8,

OSD
12, 1729–1764, 2015

top row) and then a profile that follows the similarity scaling for ε_s to the bottom, as in the case of Y01-07. With higher bottom currents above the sea floor, as for Y01-11, ε starts to increase toward values higher than $10^{-6}\,\mathrm{W\,kg^{-1}}$, similar to those observed in surface waters.

The yoyo series Y03, in contrast to Y01, presents a water column with different stratification conditions. At the beginning of the series (Fig. 9), a denser and more turbid intrusion near the bottom cause, as shown in cast Y03-02 (Fig. 8, bottom panels), a steep drop of ε to almost noise levels just above the intrusion upper limit. The presence of stronger bottom current increases ε to values in the proximity of $10^{-6}\,\mathrm{W\,kg^{-1}}$, almost reversing the damping effect of the intrusion interface and bringing back the ε profile to a distribution similar to Y02-07, in which the intrusion is not present. In Y03-18 and Y03-20, a different intrusion, with similar density but almost no turbidity (since it is clearer than previous intrusions) has a much smaller damping effect on ε.

The case of Y02 is more complex, and when compared to Y03, shows the role of buoyancy interfaces and suspended sediment concentrations in decreasing turbulence kinetic energy dissipation rates. Y02-01 has a water column with no density interface but with higher turbidity near bottom that results in a stronger damping of turbulence and low values of ε near the sea floor (Fig. 8). A similar condition is present in Y02-04 but ε_{sb} values are higher, with a strong increase of ε values near the bottom of the water column. In both these cases, there are turbidity interfaces similar to that of Y03-02 but no density interface. It has to be noted that both Y02-01 and Y02-04 present a surface density interface that dissipates some of the TKE in the first few meters of the water column, hence reducing the amount of turbulence that can penetrate to the sea floor.

A more complex ε profile can be observed in cases in which both density and turbidity interfaces are present at the bottom. In the case of Y02-06, which is subject to a surface density interface, ε decreases in the first 10 m from the surface. Then it decreases to noise levels and rises again near the sea floor following the contribution of ε_{sb}. In this case, ε is not damped by the density and turbidity interface near the sea

OSD
12, 1729–1764, 2015

floor due to the fact that in its proximity it is already near noise levels. Instead in the case of Y02-10 the surface dissipation is weaker (there is no near surface interface) and ε keeps values around $10^{-6}\,\mathrm{W\,kg^{-1}}$ up to the upper depth of the intrusion where it gets damped to values almost two order of magnitude lower. Comparison between the two profiles suggests that a strong interface (both in density and suspended sediments) damps turbulence in its vicinity. Moreover, in the case of Y02-10, ε does not increase after the interface because of higher concentration of suspended sediments, in contrast to Y03-02 that with similar ε_{sb} values but lower sediment concentration shows an increase of ε up to $10^{-6}\,\mathrm{W\,kg^{-1}}$.

The general picture that can be drawn from these results is that the water column structure (both the presence of buoyancy interface and suspended sediments) has a fundamental role to play in defining the TKE dissipation rate profiles not only in the interior of the water column but also in the proximity of the sea floor. In the specific case of the GoT, under moderate wind forcing, the presence of the intruding Adriatic Waters can be a significant limitation on complete mixing of the water column.

Due to contamination from the R/V *Urania*, the first 5 m from the sea surface was not considered in analysing the microstructure data collected. But these depths represent a fundamental part of turbulence generation and propagation since they are affected not only by wind but also by waves. In order to fully understand these processes, in future studies, this part of the water column should be investigated using a profiler rising from the bottom sufficiently far away from the ship, instead of a falling profiler deployed from the side of the vessel.

Acknowledgement. The authors thanks CNR-UPO for having allowed R/V *Urania* ship time, and the vessel crew is thanked for their kind cooperation. CARPET2014 campaign was supported by the Flagship Project RITMARE – The Italian Research for the Sea – coordinated by the Italian National Research Council and funded by the Italian Ministry of Education, University and Research within the National Research Program 2011–2013. This work was also supported by the FP7 project COCONET (Grant Agreement No: 287844) of the European Commission.

OSD
12, 1729–1764, 2015

References

Carniel, S., Sclavo, M., Kantha, L., and Prandke, H.: Double-diffusive layers in the Adriatic Sea, Geophys. Res. Lett., 35, L02605, doi:10.1029/2007GL032389, 2008.

Carniel, S., Kantha, L. H., Book, J. W., Sclavo, M., and H. Prandke: Turbulence variability in the upper layers of the Southern Adriatic Sea under a variety of atmospheric forcing conditions, Cont. Shelf Res., 44, 39–56, 2012.

Comici, C. and Bussani, A.: Analysis of the River Isonzo discharge (1998–2005), B. Geofis. Teor. Appl., 48, 435–454, 2007.

Csanady, G. T.: Circulation in the Coastal Ocean, vol 2687, Springer's edition, D. Reidel Publishing Company, Dordrecht, the Netherlands, 279 pp., 1982.

Fairall, C., Bradley, E., Hare, J., and Grachev, A.: Bulk parameterization of air–sea fluxes: updates and verification for the COARE algorithm, J. Climate, 16, 571–591, 2003.

Gargett, A. E.: "Theories" and techniques for observing turbulence in the euphotic zone, Sci. Mar., 6, 24–45, 1997.

Malačič, V. and Petelin, B.: Gulf of Trieste, in: Physical Oceanography of the Adriatic Sea, Past, Present and Future, edited by: Cushman-Roisin, B., Gačić, M., Poulain, P.-M., and Artegiani, A., Kluwer Academic Press, Dordrecht, the Netherlands, 167–177, 2001.

Malačič, V .M., Celio, M., and Naudin, J. J.: Dynamics of the surface water in the Gulf of Trieste (Northern Adriatic) during drifting experiments, in: The Adriatic Sea, edited by: Hopkins, T. S., Artegiani, A., Cauwet, G., Degobbis, D., and Malej, A., Ecosystem Research Report No. 32, EUR 18834, European commission, Brussels, 117–125, 1999.

Malačič, V., Petelin, B., and Vodopivec, M.: Topographic control of wind-driven circulation in the northern Adriatic, J. Geophys. Res., 117, C06032, doi:10.1029/2012jc008063, 2012.

Peters, H. and Orlić, M.: Turbulent mixing in the springtime central Adriatic Sea, Geofizika, 22, 1–19, 2005.

Peters, H., Craig, M. L., Orlić, M., and Dorman, C. E.: Turbulence in the wintertime northern Adriatic Sea under strong atmospheric forcing, J. Geophys. Res., 112, C03S09, doi:10.1029/2006JC003634, 2007.

Querin, S., Crise, A., Deponte, D., and Solidoro, C.: Numerical study of the role of wind forcing and freshwater buoyancy input on the circulation in a shallow embayement (Gulf of Trieste, Northern Adriatic Sea), J. Geophys. Res., 111, C03S16, doi:10.1029/2006JC003611, 2006.

Raicich, M.: On the fresh water balance of the Adriatic Sea, J. Marine Syst., 9, 305–319, 1996.

OSD
12, 1729–1764, 2015

Ricchi, A., Miglietta, M. M., Falco, P. P., and Carniel, S.: On the use of a coupled ocean–atmosphere–wave model during an extreme Cold Air Outbreak over the Adriatic Sea, Atmos. Res., in review, 2015.

Shay, T. J. and Gregg, M. C.: Turbulence in an oceanic convective mixed layer, Nature, 310, 282–285, 1984.

Shay, T. J. and Gregg, M. C.: Convectively driven turbulent mixing in the upper ocean, J. Phys. Oceanogr., 16, 1777–1798, 1996.

Sinjur, I., Vertačnik, G., Likar, L., Hladnik, V., Miklavčič, I., and Gustinčič, M.: Ice storm in Slovenia in January and February 2014 – spatial and temporal variability in weather across the dinaric landscapes in Slovenia, Gozdarski vestnik, 72, 299–309, 2014 (in Slovenian, abstract and discussion in English).

Thorpe, S. A.: Recent developments in the study of ocean turbulence, Annu. Rev. Earth Pl. Sc., 32, 91–109, 2004.

OSD
12, 1729–1764, 2015

Table 1. BIAS, Root Mean Square Error (RMSE) and Percentual RMSE computed for the ISMAR and NIB MSS probes compared to CTD measurements.

	BIAS	RMSE	PRMSE
ISMAR – Temperature	0.0046	0.0205	0.1932
ISMAR – Salinity	−0.2418	0.2424	0.6517
NIB – Temperature	−0.0072	0.0280	0.2530
NIB – Salinity	0.0300	0.2227	0.0607

OSD
12, 1729–1764, 2015

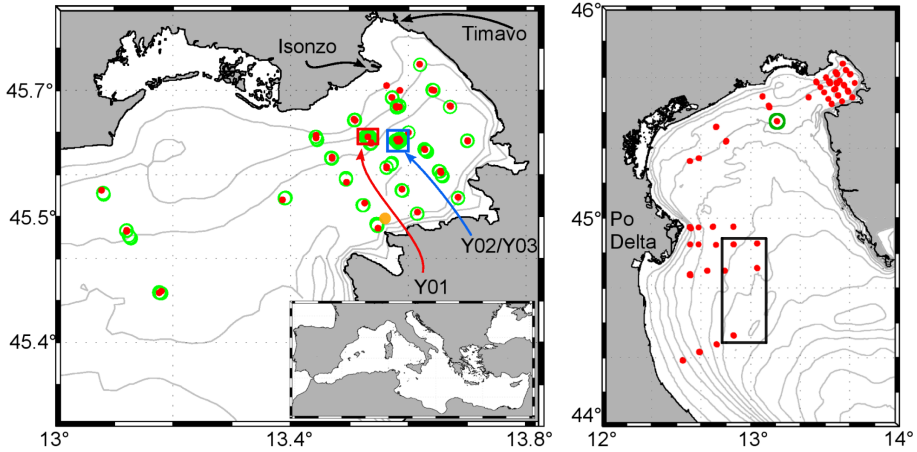

Figure 1. Left panel shows the location of the CARPET2014 stations inside the GoT. Red dots denote CTD stations; green circles MSS stations, red and blue squares MSS yoyo sites fro Y01 and Y02/Y03 respectively; yellow dot points the VIDA buoy. The insert shows the location of the Adriatic Sea inside the Mediterranean Sea. Right panel shows stations of the entire CARPET2014 cruise. Red dots show locations of CTD casts; black square marks the area of the CTD casts considered representative of open sea waters (see Fig. 5), the green circle shows the station used as Y02 and Y03 end points.

OSD
12, 1729–1764, 2015

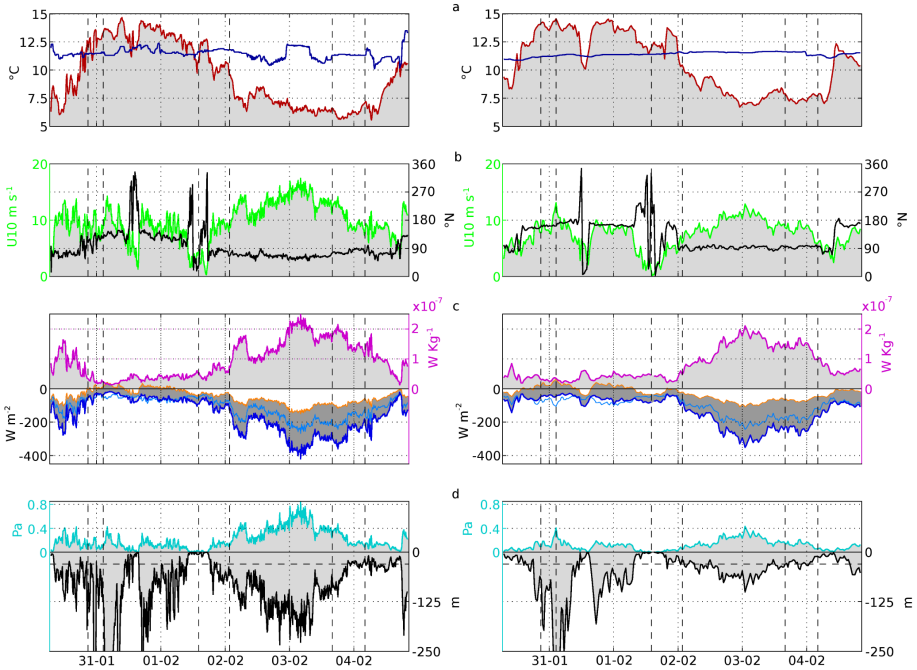

Figure 2. Atmospheric and sea surface observations and fluxes collected from the R/V *Urania* (left panels) and VIDA buoy (right panels). **(a)** Air (Tair, red) and sea (Tsea, blue) temperature time series; **(b)** wind speed (green) and wind direction (black); **(c)** net (J_{to}, blue line), latent (J_l, light blue) and sensible (J_s, orange) heat fluxes computed with the COARE algorithm and buoyancy flux (J_b, magenta); **(d)** wind stress (τ, cyano) and Monin–Obukhov length (L_{mo}, black). Given that the maximum depth of the GoT is 25 m the L_{mo} is shown up to 250 m depth to provide a clearer representation of the water column. L_{mo} values can be as much as 1200 m during the calm periods. Vertical dashed lines show the yoyo cast collection time.

OSD
12, 1729–1764, 2015

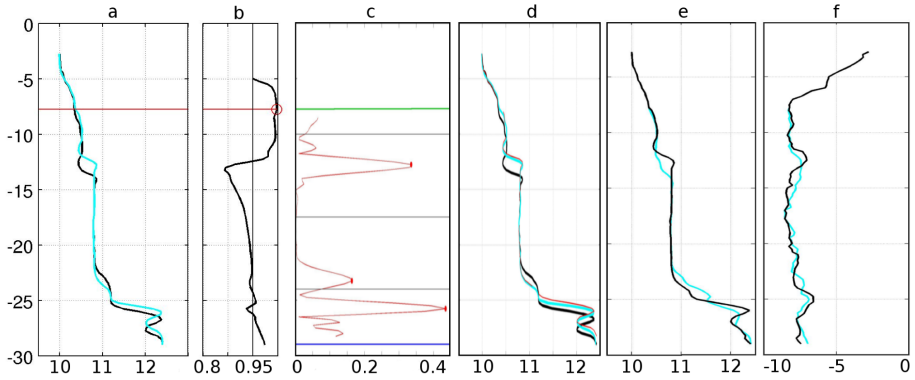

Figure 3. Panel **(a)** shows temperature profiles: reference in cyan, profile to be realigned in black. Panel **(b)** shows correlation coefficient computed for progressively longer segments starting form surface. The black vertical line is the 0.95 correlation threshold and the red circle the maximum correlation. Panel **(c)** shows root mean square error between the two profiles; red dots identify peaks. Black horizontal lines divide the segments used for realignment. Panel **(d)** shows the realigned segments (thin red lines) above the two original profiles (same colours as in panel **a**). Panels **(e)** and **(f)** show the mean profile for temperature and turbulent kinetic energy dissipation rates computed using the original profiles (cyan) and the realigned ones (black).

OSD
12, 1729–1764, 2015

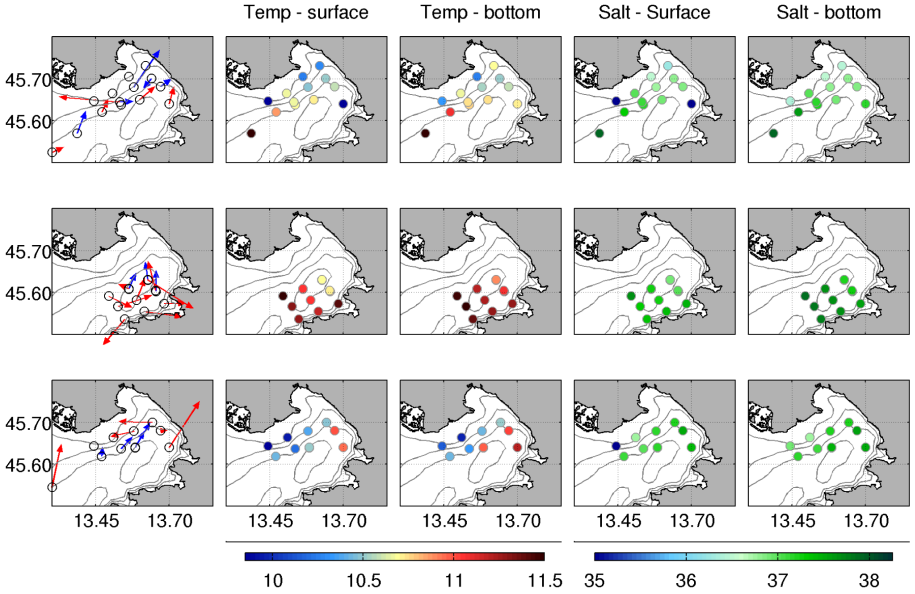

Figure 4. Bottom currents and values from CTD casts at certain depths are shown inside the GoT for 30 January (top panels), 31 January (central panels) and 4 February (bottom panels). Panels on the left column show the ADCP bottom cell currents; red arrows are observations taken during rising tide, blue arrows during falling tide. Temperature (second and third columns) and salinity (fourth and fifth columns) values for surface (0 and 2.5 m) and bottom layers (last 2.5 m of cast) inside the GoT.

OSD
12, 1729–1764, 2015

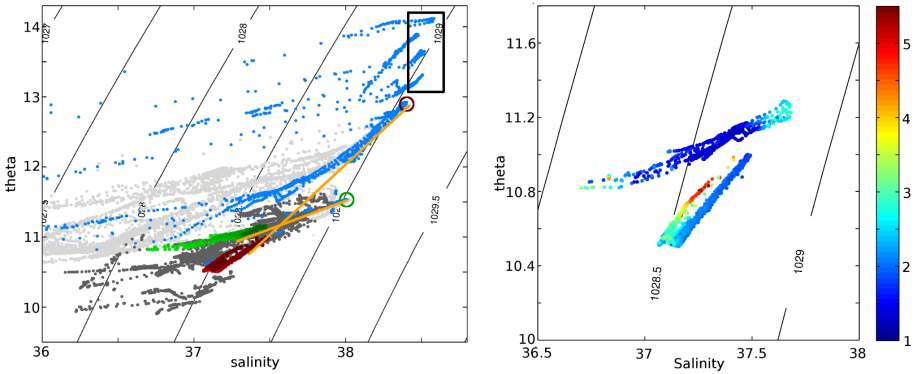

Figure 5. Left panel shows θ–S plot of all CTDs and MSSs (both ISMAR and NIB) observations (light grey for the Northern Adriatic and dark grey for the GoT). The green and red dots are the MSS-ISMAR and MSS-NIB ensemble means for Y02 and Y03 respectively, light colour for surface values and dark colour for bottom ones. The green circle indicates the bottom waters observed at the entrance of the GoT on 30 January that are the end point for Y02 bottom waters; Red circles point to deep waters outside the GoT on 4 January considered as the end point of Y03 bottom water. The black square encompasses values in bottom waters in the centre of the North Adriatic Sea. Locations of end points are shown in Fig. 1. The profiles of the cast leading to the end points are shown in light blue. Right panel shows θ–S plot for Y02 and Y03. Colour scale shows turbidity FTUs as measured by the back scatterometer mounted on the MSS ISMAR probe.

OSD
12, 1729–1764, 2015

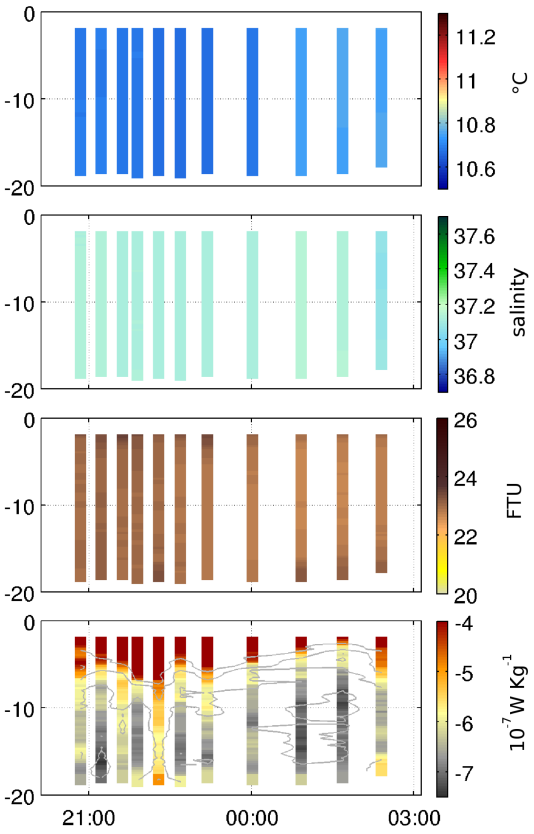

Figure 6. Hovmöller diagrams for Y01: **(a)** temperature profiles; **(b)** salinity profiles; **(c)** turbidity profiles in FTU; **(d)** turbulent kinetic energy dissipation rate (contours spaced 1 W Kg^{-1}). Red dashed lines show the time of collection of the Y01 casts reported in top panels of Fig. 8.

OSD
12, 1729–1764, 2015

Turbulence observations in the Gulf of Trieste

F. M. Falcieri et al.

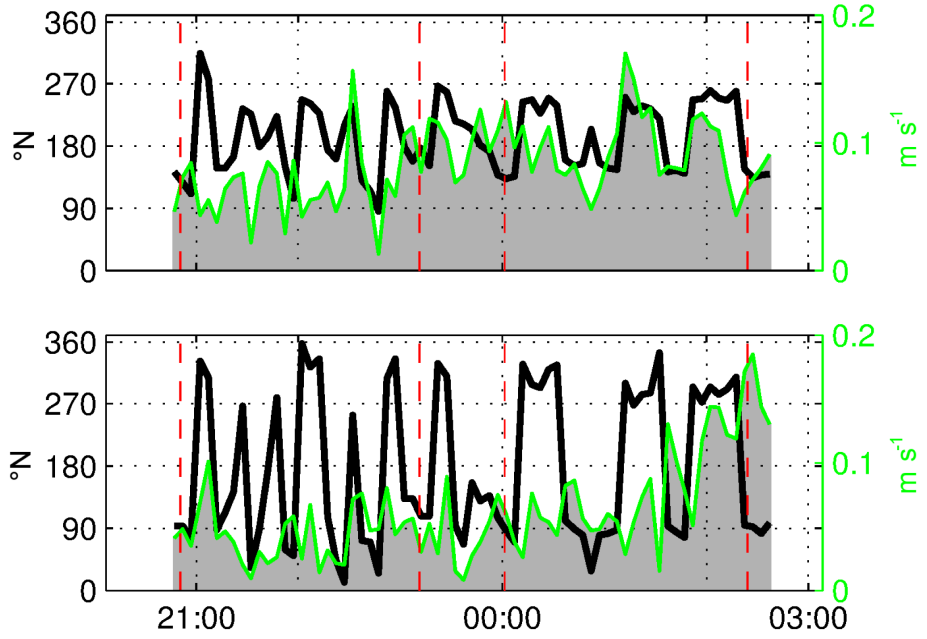

Figure 7. Second (top panel) and third (bottom panels) cells of Y01 ADCP currents. The cell centres are located at 13 and 17 m below sea surface; cell width is 4 m. Black lines show current direction in degrees (due north) and green lines show current magnitude in m s^{-1}. Red dashed lines show the time of collection of the Y01 casts reported in top panels of Fig. 8.

OSD
12, 1729–1764, 2015

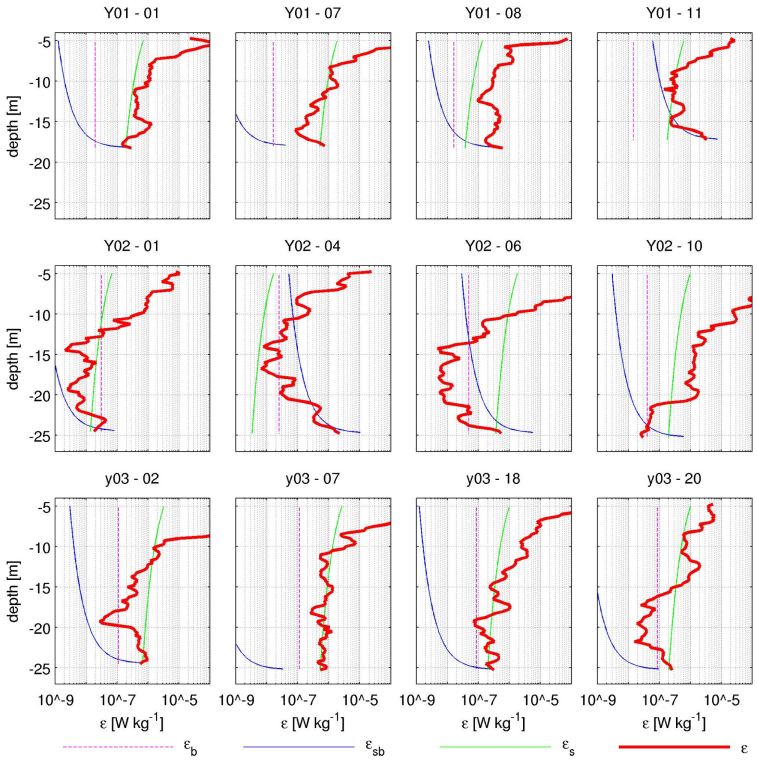

Figure 8. Similarity scaling of turbulent kinetic energy dissipation rate (ε) for four representative casts for each yoyo, Y01 top panels, Y02 central panels and Y03 bottom panels. For each cast is shown the observed TKE dissipation rate (ε, thick red line), and the turbulence generated by surface wind stress (ε_s, green line), bottom shear stress (ε_{sb}, blue line) and buoyancy flux (ε_b, magenta vertical dashed line).

OSD
12, 1729–1764, 2015

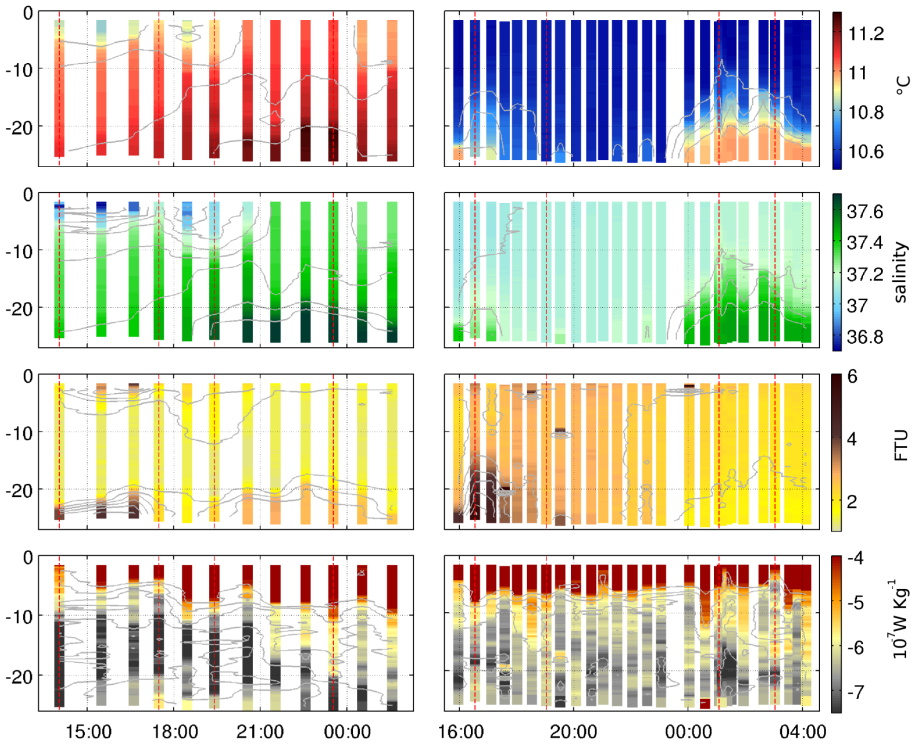

Figure 9. Hovmöller diagrams of Y02 (left) and Y03 (right). Panels shows: **(a)** temperature profiles (grey contours are spaced 0.1 °C); **(b)** salinity profiles (grey contours are spaced 0.1 PSU); **(c)** turbidity profiles in FTU (grey contours are spaced 1FTU); **(d)** turbulent kinetic energy dissipation rate (contours spaced 1 $W m^{-2}$). Red dashed lines show the time of collection of the Y01 casts reported in top panels of Fig. 8.

OSD
12, 1729–1764, 2015

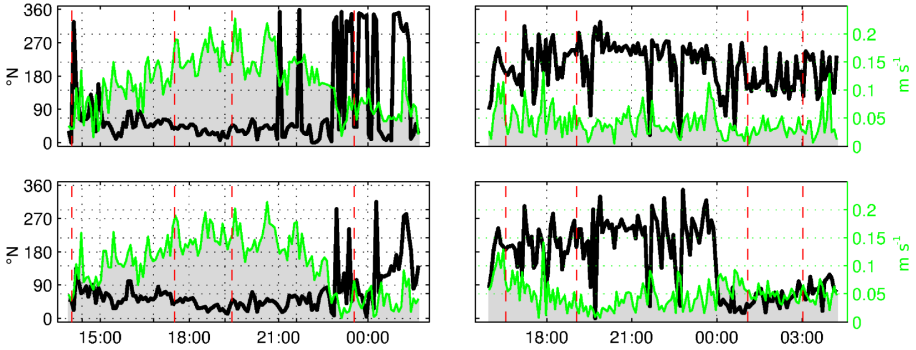

Figure 10. Second (top panel) and third (bottom panels) cells of ADCP currents. The cell centres are located at 13 and 17 m below sea surface; cell width is 4 m. Black lines show current direction (due north) and green lines show current magnitude in m s^{-1}. Left panels show Y02, right panels Y03. Red dashed lines show the time of collection of the Y01 casts reported in top panels of Fig. 8.

OSD
12, 1729–1764, 2015